MOLECULAR AND CELLULAR BIOLOGY, Apr. 2011, p. 1551–1564 Vol. 31, No. 7
0270-7306/11/$12.00 doi:10.1128/MCB.00834-10

Tctex-1, a Novel Interaction Partner of Rab3D, Is Required for Osteoclastic Bone Resorption▽

Nathan J. Pavlos,[1] Tak Sum Cheng,[1]† An Qin,[1,2]† Pei Ying Ng,[1] Hao-Tian Feng,[1] Estabelle S. M. Ang,[1] Amerigo Carrello,[1] Ching-Hwa Sung,[3] Reinhard Jahn,[4] Ming-Hao Zheng,[1]* and Jiake Xu[1]*

Centre for Orthopaedic Research, School of Surgery, University of Western Australia, Perth 6009, Western Australia, Australia[1]; Department of Orthopaedics, Ninth People's Hospital, Shanghai Jiao Tong University, School of Medicine, Shanghai 200011, China[2]; Departments of Ophthalmology and Cell and Developmental Biology, Weill Medical College of Cornell University, Ithaca, New York[3]; and Department of Neurobiology, Max Planck Institute for Biophysical Chemistry, Göttingen 37077, Germany[4]

Received 19 July 2010/Returned for modification 31 August 2010/Accepted 28 December 2010

Vesicular transport along microtubules must be strictly regulated to sustain the unique structural and functional polarization of bone-resorbing osteoclasts. However, the molecular mechanisms bridging these vesicle-microtubule interactions remain largely obscure. Rab3D, a member of the Rab3 subfamily (Rab3A/B/C/D) of small exocytotic GTPases, represents a core component of the osteoclastic vesicle transport machinery. Here, we identify a new Rab3D-interacting partner, Tctex-1, a light chain of the cytoplasmic dynein microtubule motor complex, by a yeast two-hybrid screen. We demonstrate that Tctex-1 binds specifically to Rab3D in a GTP-dependent manner and co-occupies Rab3D-bearing vesicles in bone-resorbing osteoclasts. Furthermore, we provide evidence that Tctex-1 and Rab3D intimately associate with the dynein motor complex and microtubules in osteoclasts. Finally, targeted disruption of Tctex-1 by RNA interference significantly impairs bone resorption capacity and mislocalizes Rab3D vesicles in osteoclasts, attesting to the notion that components of the Rab3D-trafficking pathway contribute to the maintenance of osteoclastic resorptive function.

Osteoclasts are terminally differentiated polykaryons whose exclusive function is the degradation of mineralized bone matrix (45). Excessive osteoclast numbers and/or activity manifests in many pathological osteolytic disorders, including Paget's disease, multiple myeloma, and osteoporosis (55). These multinucleated cells mature from the asynchronous fusion of mononuclear precursors of the monocyte/macrophage lineage, a process orchestrated by two principal osteoclastogenic cytokines, namely, macrophage colony-stimulating factor (M-CSF) and receptor activator of nuclear factor kB (RANK) ligand (RANKL).

Upon attachment to bone, osteoclasts undergo a defined program of cytoskeletal and membrane reorganizations which culminate in the segregation of their plasmalemma into four distinct domains: (i) the ruffled border, (ii) the sealing zone, (iii) the basolateral domain, and (iv) the functional secretory domain (5, 30, 53, 57). The sealing zone is circumscribed by a tight ring of a filamentous actin which serves as a site of osteoclast attachment and seals off the underlying resorptive space. Adjacent to the bone surface and limited by the sealing zone, the ruffled border membrane presents the resorptive organelle and serves as an exit site for protons and osteolytic enzymes (e.g., cathepsin K) as well as an uptake zone for the removal of degraded osseous tissue. Thus, vesicular trafficking must be tightly coupled to the osteoclastic cytoskeleton in order to sustain the specialized structural and functional polarization of the ruffled border and basolateral domains. In recent years, several components of the osteoclast vesicle transport machinery have been unveiled (1, 32, 41, 50, 58, 59). Among these, small Ras-related Rab GTPases (40, 56) have emerged as key regulators of ruffled border formation and function.

We have previously shown that Rab3D, a member of the exocytotic subfamily of Rab3 GTPases (Rab3A/B/C/D), regulates a post-*trans*-Golgi network (TGN) trafficking step that is required for the maintenance of the ruffled border membrane (32). Moreover, mice lacking Rab3D were found to exhibit an osteosclerotic (high-bone-mass) phenotype, owing to defective osteoclasts which have abnormal ruffled borders, consistent with a defect in vesicular trafficking. While these findings clearly implicate an important role for Rab3D in vesicle delivery and membrane insertion at the ruffled border, the complement of molecular effectors through which it exerts its regulatory activity remains unknown.

To address this issue, we employed a yeast two-hybrid (Y-2H) system to screen for Rab3D binding proteins. Herein, we identify Tctex-1, a light chain of the microtubule dynein motor complex, as a candidate Rab3D-interacting partner and discuss the functional implications of this novel interaction during osteoclastic bone resorption.

* Corresponding author. Mailing address: 2nd Floor M Block QEII Medical Centre, Nedlands, Perth, Western Australia 6009, Australia. Phone: 61 (8) 9346-3213. Fax: 61 (8) 9346-3210. E-mail for Jiake Xu: jiake.xu@uwa.edu.au. E-mail for Ming-Hao Zheng: minghao.zheng@uwa.edu.au.

† These authors contributed equally to the work.

▽ Published ahead of print on 24 January 2011.

MATERIALS AND METHODS

Antibodies. Rabbit polyclonal antibodies against Tctex-1 were generously provided by S. M. King (20). Generation and characterization of a monoclonal anti-Tctex-1 antibody and polyclonal rabbit anti-Rab3D antibodies used in this

study have been described previously (32, 34, 42). The other antibodies used were mouse anti-dynein intermediate chain (IC74) (Chemicon), goat anti-human Rab3D (Santa Cruz Biotechnology), rabbit anti-vesicular glutamate transporter 1 (VGLUT-1) (Synaptic Systems), mouse anti-Myc (Synaptic Systems), rabbit anti-green fluorescent protein (GFP) (Synaptic Systems), mouse anti-chicken α-tubulin (Sigma), and mouse anti-FLAG M2 (Invitrogen). Alexa Fluor 546- and 488- and horseradish peroxidase (HRP)-conjugated goat anti-mouse immunoglobulin G (IgG), goat anti-rabbit IgG, sheep anti-goat IgG, and goat anti-chicken IgG were all purchased from Invitrogen. All antibodies were used at the concentrations recommended by the supplier.

Two-hybrid screening and mapping studies. A pVP16-based yeast two-hybrid cDNA library was kindly provided by S. P. Klinken (Western Australian Institute for Medical Research). Murine Rab3D-N (amino acids [aa] 1 to 151) and Rab3D-C (aa 151 to 219) terminal plasmid baits were generated by PCR and cloned into pBTM116 yeast expression vectors containing the LexA reporter gene. For cDNA library screening, the baits were introduced in the yeast reporter strain L40 together with the pVP16 mouse embryo cDNA library (prey) using lithium acetate and polyethylene glycol. Library plasmids that grew on minimal agar plates lacking histidine (His^-) were screened for LacZ activity using standard β-galactosidase activity assays (38). Positive clones isolated from the cDNA library were further confirmed by isolating clone inserts and reintroducing them into the yeast strain with the baits and screening for growth. For mapping studies, truncated forms of Rab3D cDNA (encoding Rab3D aa 1 to 74, aa 74 to 95, aa 74 to 219, aa 1 to 151, and aa 95 to 219) were cloned into pBTM116 vectors and cotransformed with pVP16-Tctex-1 into the L40 reporter strain and analyzed for His^+ activity and β-galactosidase activity. Similarly, pVP16-Tctex-1 was cotransformed with the pBTM116 LexA-fused Rab3D, Rab3C, Rab5, Rab5N-35, Rab5L-7a, or Rab6L72 plasmid and screened for His^+ reporter activation. cDNAs encoding Rab5, Rab5N-35, Rab5L-7a, and Rab6L72 were generously provided by M. Zerial and H. Stenmark (Max Planck Institute of Molecular Cell Biology and Genetics).

Expression plasmid construction. The complete cDNA encoding murine Tctex-1 cDNA was PCR amplified from the pVP16 vector used in the Y-2H screen and subcloned into the pGEX-3X bacterial expression vector. Mammalian expression constructs containing Myc-tagged Rab3A, Rab3B, Rab3C, and Rab3D cDNAs were generously provided by R. Regazzi (13). C-terminal FLAG-tagged Tctex-1 was a kind gift from K. S. Campbell (3). A FLAG-tagged Rab3D vector was generated by subcloning the full-length mouse Rab3D cDNA into a pcDNA 3.1 mammalian expression vector containing a FLAG epitope. The generation of enhanced yellow fluorescent protein (EYFP)-tagged Rab3Dwt, $Rab3D^{Q81L}$, $Rab3D^{N135I}$, and $Rab3D^{\Delta CXC}$ cDNA constructs has previously been described (32). An EYFP-fused Rab3Awt expression plasmid was constructed by subcloning the full-length mouse Rab3A cDNA into a pcDNA 3.1 vector containing an EYFP. An EGFP-Rab7 vector was kindly provided by B. van Duers (2).

Cell culture and transfections. COS-1 and RAW 264.7 cells were grown per American Type Culture Collection guidelines in either Dulbecco's modified Eagle's medium (DMEM) or α-modified MEM (α-MEM) supplemented with 10% fetal calf serum (FCS). Plasmid transfections used Lipofectamine 2000 (Invitrogen) according to the manufacturer's instructions. All cell cultures were maintained in 5% CO_2 at 37°C.

Expression, isolation, and pulldown of GST–Tctex-1. Expression of glutathione *S*-transferase (GST)–Tctex-1 was performed essentially as described in reference 54. To express FLAG-Rab3D, ~5×10^5 COS-1 cells were transfected with 10 μg of FLAG-Rab3D plasmid for 2 days, after which cells were washed with ice-cold PBS and lysed on ice with 750 μl of lysis buffer (50 mM Tris-Cl [pH 7.5], 150 mM NaCl, 0.1% Nonidet P-40, 0.7 μg/ml pepstatin). Following centrifugation at 12,000 rpm for 5 min at 4°C, supernatant was collected and 750 μl of binding buffer (20 mM Tris-Cl [pH 7.5], 50 mM KCl, 100 mM NaCl, 2 mM $CaCl_2$, 2 mM $MgCl_2$, 5 mM dithiothreitol [DTT]) was added to the supernatant and mixed. One half of the sample was added to 10 μg of GST protein alone immobilized in glutathione agarose beads and the other to 10 μg of the GST–Tctex-1 fusion protein. The mixture was incubated overnight at 4°C, and then the beads were washed with lysis buffer and binding buffer. The bound proteins were analyzed by SDS-PAGE and immunoblotting using anti-FLAG M2 monoclonal antibodies.

Immunoprecipitations and immunoblotting. COS-1 cells (~2×10^6) transfected with 2 μg each of pFLAG–Tctex-1 and pcDNA 3.1 plasmid vector DNA encoding either full-length Myc-tagged wild-type Rab3A, Rab3B, Rab3C, and Rab3D or EYFP-tagged $Rab3D^{wt}$, $Rab3D^{Q81L}$, and $Rab3D^{N135I}$ fusion chimeras were washed with ice-cold phosphate-buffered saline (PBS) and scraped with 400 μl of lysis buffer (50 mM HEPES-KOH [pH 7.2], 150 mM NaCl, 1 mM $MgCl_2$) supplemented with protease inhibitors (1 mM phenylmethylsulfonyl fluoride [PMSF], 1 μg/ml aprotinin, 1 μg/ml leupeptin, and 0.7 μg/ml pepstatin [all from Sigma]), and then homogenized by passing cells through a 25-gauge syringe (at least 10 strokes). Proteins were then cleared by centrifugation at 3,000 rpm for 15 min at 4°C. The resulting postnuclear supernatants (PNS) were divided into equal volumes (200 μl), supplemented with either GDP or GTP[γS] (guanosine 5′-*O*-[3-thiotriphosphate]) (both from Sigma), adjusted with Triton X-100 to 1%, and solubilized for 1 h at 4°C. Insoluble material was removed by centrifugation 15 min at 16,000 × g at 4°C, and either Myc-Rab3 proteins or FLAG–Tctex-1 proteins were immunoprecipitated overnight with monoclonal anti-Myc, anti-FLAG M2, or IgG control antibodies at 4°C. Immunocomplexes were captured with 30 μl of protein G-Sepharose 4 Fast Flow (GE Healthcare) for 2 h at 4°C and washed with lysis buffer containing 0.2% Triton X-100. Immunoprecipitates were analyzed by SDS-PAGE and immunoblotting with anti-FLAG M2, anti-Myc, and anti-GFP antibodies. For immunoblotting, lysates and protein-immune complexes diluted in SDS sampling buffer were boiled, resolved by SDS-PAGE (10 to 15% polyacrylamide gels), and blotted onto nitrocellulose membranes (Hybond ECL; Amersham Life Science). Following transfer, membranes were blocked with 5% skim milk in Tris-buffered saline-Tween 20 (TBS-T) for 40 min and then probed with primary antibodies diluted in 1% (wt/vol) skim milk powder in TBS-T for 2 h. Membranes were washed, incubated with HRP-conjugated secondary antibodies, and developed using the enhanced chemiluminescence (ECL) detection system (Amersham).

GTP binding and BRET assay. Binding of [α-P^{32}]GTP to proteins blotted on nitrocellulose membrane was carried out as previously described (32). Bioluminescence resonance energy transfer (BRET) assays were performed as described in reference 7, with minor modifications. In brief, the complete cDNA encoding murine Tctex-1 was fused to the *Renilla* luciferase (Rluc) donor fluorophore contained within a pcDNA 3.1 mammalian expression vector. COS-1 cells were transiently cotransfected with pRluc–Tctex-1 and an EYFP-fused (acceptor fluorophore) construct encoding $Rab3D^{wt}$, $Rab3D^{Q81L}$, $Rab3D^{N135I}$, $Rab3D^{\Delta CXC}$, and $Rab3A^{wt}$ or EYFP alone (negative control) for 2 days, after which coelenterazine (5 μM, H form; Invitrogen) was added and repeated BRET readings were immediately collected within 440- to 500- (Rluc) and 510- to 590- (EYFP) nm windows using a Mithras LB940 BRET plate reader (Berthold Technologies, Inc., Germany). The BRET ratio was defined as [(emission at 510 to 590 nm) − (emission at 440 to 500 nm) × *cf*]/(emission at 440 to 500 nm), where *cf* corresponds to (emission at 510 to 590 nm)/(emission at 440 to 500 nm) for the Rluc construct expressed alone in the same experiment. Where indicated, cells cotransfected with pRluc–Tctex-1 and pEYFP-Rab3Dwt were treated with vehicle (dimethyl sulfoxide [DMSO]), cytochalasin D (cyto D; 1 μM; Sigma), brefeldin A (BfA; 6 μg/ml; Sigma), or nocodazole (Noc; 6 μg/ml; Sigma) prior to measuring BRET signals.

Sequence and structural alignment. Primary sequence alignments were performed by using ClustalW. Protein structures were modeled with Swiss-Pdb-Viewer.

Generation and isolation of OCLs. Osteoclastic cells were generated using two established pro-osteoclastic systems. The first utilized RAW 264.7 cells, an M-CSF-independent murine monocyte-macrophage cell line shown to support the differentiation of osteoclast-like cells (OCLs) in the presence of RANKL (100 ng/ml) (54). The second employed either bone marrow macrophages (BMMs) or human peripheral blood monocytes (PBMCs) differentiated with RANKL (100 ng/ml) and M-CSF (25 ng/ml) as previously described (32). For the isolation of mature primary human osteoclasts, cells were mechanically disaggregated from osteoclastoma tissue (giant cell tumor of bone) according to methods outlined in reference 12. Osteoclastoma tissue, sourced from 2 independent cases, was collected fresh from patients postoperatively (Sir Charles Gairdner Hospital, Nedlands, WA, Australia). All patients consented, and experiments were approved by a Human Ethics Committee, The University of Western Australia. Cells were harvested and processed for total RNA extraction, velocity density gradient centrifugation, and immunoblot analysis or seeded onto either glass coverslips or devitalized cortical bovine bone surfaces before being fixed and processed for immunofluorescence microscopy.

RT-PCR. Total RNA was isolated from OCLs using RNAzol solution according to the manufacturer's instructions (Ambion Inc.). For reverse transcription (RT)-PCR, cDNA was prepared from 2 μg of total RNA using reverse transcriptase with an oligo(dT) primer. All PCRs were carried out using 2 μl of each cDNA using the following cycling parameters: 94°C, 45 s; 54°C, 45 s; and 72°C, 45 s for 30 cycles (except the calcitonin receptor [CTR] whose annealing temperature was 60°C). Primers (designed against the indicated mouse sequences) for Rab3D (forward, 5′-ATGGCATCCGCTAGTGAG-3′; reverse 5′-CTAACAGCTGCAGCTGCT-3′), Tctex-1 (forward, 5′-ATGCGTTAAAGATGGAAGACTTC-3′; reverse, 5′-TCAGATGGACAGTCCGAAGG-3′), CTR (forward, 5′-TGGTTGAGGTTGTGCCCA-3′; reverse, 5′-CTCGTGGGTTTGCCTCATC-3′), and acidic ribosomal phosphoprotein (36B4) (forward, 5′-TCATTGTGGG

AGCAGACA-3′; reverse, 5′-TCCTCCGACTCTTCCTTT-3′), which served as an internal control, were used. Ten microliters of each PCR product was separated on a 1.5% agarose gel containing ethidium bromide and photographed.

siRNA-mediated Tctex-1 knockdown, bone resorption assays, and medium CTx-1 measurements. Silencer predesigned small interfering RNAs (siRNAs) directed against human Tctex-1 (denoted TC1 to TC3) and nontargeting control siRNAs (negative and GFP) were purchased from Ambion: Tctex-1 siRNA TC1 (siRNA ID no. 18162), Tctex-1 siRNA TC2 (siRNA ID no. 139626), Tctex-1 siRNA TC3 (siRNA ID no. 139627), negative-control siRNA (Silencer negative control no. 1 siRNA), and GFP siRNA (Silencer GFP [eGFP] siRNA). For siRNA experiments, 100 nm of Tctex-1-directed or control siRNAs were transfected into osteoclastic cells using HiPerfect transfection reagent (Qiagen) in accordance with the manufacturer's protocol and level of mRNA and/or protein suppression analyzed by semiquantitative RT-PCR and immunoblotting after 48 h posttransfection. For osteoclastogenesis experiments, MCSF-dependent monocytes isolated from human peripheral blood (PBMCs) were transfected with siRNA and stimulated with 100 ng/ml RANKL on days 1, 3, and 6 of osteoclast formation. After 10 days of culture, osteoclast-like cells were stained for tartrate-resistant acid phosphatase (TRACP) activity, and numbers of osteoclastic cells with more than 5 nuclei were quantified. To assess bone resorption activity, PBMCs were induced to form osteoclasts with 100 ng/ml RANKL and 25 ng/ml M-CSF. Mature PBMC-derived osteoclasts were seeded onto bovine bone slices and silenced as described above for 48 h, after which the culture media were collected, osteoclasts were fixed with 4% paraformaldehyde and stained for TRACP activity, and resorption pits visualized by scanning electron microscopy (SEM) and surface texture profilometry using the Zygo NewView 6300 3D optical profilometer (Zygo Corporation, CT). Resorption pit depth and volume were analyzed using MetroPro Advance Texture software (Zygo Corporation, CT). Medium CTx-1 levels were determined using the CrossLaps for culture ELISA kit (Immunodiagnostic Systems) according to the manufacturer's instructions.

Velocity density gradient centrifugation and immunoprecipitation of Rab3D-Tctex-1 complexes in osteoclastic cells. Velocity density gradient centrifugation was performed as previously described in reference 19, with minor modifications. Briefly, $\sim 3 \times 10^7$ osteoclastic cells were pelleted, and cell extracts were prepared as described in "Immunoprecipitations and immunoblotting." A total of 500 μl of the clarified supernatant was layered on top of 12 ml of 5 to 20% linear sucrose density gradient prepared in the lysis buffer without Triton X-100. After centrifugation at 150,000 × *g* for 18 h in an SW40 rotor (Beckman Coulter), 1-ml fractions were collected and analyzed by immunoblotting using antibodies to Rab3D, Tctex-1, IC74, and α-tubulin. For the immunoprecipitation of endogenous Rab3D–Tctex-1 complexes, peak Rab3D–Tctex-1 fractions were pooled, supplemented with GTP[γS] (0.5 mM), and immunoprecipitated overnight with either anti-Rab3D or IgG control antibodies essentially as described above. Immunocomplexes were captured with protein G-Sepharose 4 Fast Flow (GE Healthcare), washed, and resolved by SDS-PAGE and immunoblotting with antibodies against Rab3D and Tctex-1.

Immunofluorescence confocal microscopy. For immunofluorescent staining, human osteoclasts cultured on glass coverslips or devitalized cortical bovine bone discs were fixed with either 4% paraformaldehyde (PFA) in PBS for 15 min at room temperature and permeabilized for 5 min with 0.1% Triton X-100 in PBS or methanol (−20°C) for 10 min. In some instances, osteoclasts were preincubated with microtubule stabilizing buffer (MTSB) {80 mM PIPES [piperazine-*N*,*N*′-bis(2-ethanesulfonic acid)] [pH 6.8], 1 mM $MgCl_2$, 4 mM EGTA} supplemented with 0.5% Triton X-100 for 30 s at room temperature prior to methanol fixation or with 0.02% saponin to release free cytosolic dynein and Rab protein, respectively. Nonspecific binding of antibodies was blocked by 10% FCS in PBS for 30 min, after which cells were incubated with primary antibody diluted in 0.2% bovine serum albumin (BSA)-PBS for 1 h at room temperature. Following extensive washing, bound primary antibodies were visualized with Alexa Fluor secondary antibody conjugates (Invitrogen). Where indicated, osteoclasts were incubated with media containing either vehicle (DMSO) or the microtubule depolymerizing agent nocodazole (6 μg/ml; Sigma) for 2 h. Hoechst 3342 dye (Invitrogen) was used to visualize cell nuclei. In some instances, siRNA-treated human osteoclasts seeded on bovine bone slices were immunostained for rhodamine-conjugated phalloidin (Invitrogen) and anti-Rab3D antibodies to monitor sealing zone/ruffled border formation and Rab3D localization, respectively. Detection of fluorochromes was carried out with a confocal laser scanning microscope (CLSM) (MRC-1000; Bio-Rad), equipped with 40× (UV, numerical aperture [NA] of 1.2) and 60× (NA of 1.6) oil immersion lenses (all Nikon). Confocal sequences were collected as Bio-Rad PIC files and were converted to bitmaps for use in Image J (NIH).

Statistics and data presentation. Results were statistically analyzed using a two-tailed Student *t* test using GraphPad Prism version 3.00 (GraphPad Software). All data shown represent one of at least three independent experiments.

RESULTS

Identification of Tctex-1 as a Rab3D binding protein. To identify candidate Rab3D-interacting proteins, we performed a yeast two-hybrid (Y-2H) screen of a randomly primed mouse embryo cDNA library using the N terminus of murine Rab3D as "bait." This approach yielded 100 histidine/LacZ-positive ($His^+/LacZ^+$) clones from approximately 75×10^6 cotransformants. Among these, five independent clones (M18, M30, M37, M39, and M40) were identified that carried the open reading frame *Tctex-1* (t-complex testis-expressed-1), also designated the DYNLT1 gene (33), encoding a 14-kDa light chain of the minus-end microtubule motor complex cytoplasmic dynein (20) (Fig. 1A and B). Further Y-2H analyses revealed that Tctex-1 specifically interacted with members of the Rab3 GTPase subfamily (Rab3C/D, Fig. 1C) but not other Rab family proteins tested, including Rab5 and Rab6 (Fig. 1C). The specificity of this Rab3D–Tctex-1 binding was verified biochemically by *in vitro* glutathione *S*-transferase (GST)-pull-down assays using purified recombinant GST–Tctex-1. As shown in Fig. 1D, immunobilized GST–Tctex-1, but not GST alone (negative control), efficiently recovered FLAG-tagged Rab3D from transfected cell lysates, indicating that Rab3D forms a complex with Tctex-1.

To map the regions of Rab3D that are required for Tctex-1 interaction, we next generated a series of Rab3D deletion constructs and tested their ability to interact with Tctex-1 by Y-2H analysis (Fig. 1E and F). Whereas full-length Rab3D and amino acid truncations (aa 1 to 151 and aa 74 to 219) of Rab3D exhibited strong interactions with Tctex-1, amino acid deletions (aa 1 to 74 and 95 to 219) completely abrogated this association, suggesting that amino acids 74 to 95 were both sufficient and required for binding between Rab3D and Tctex-1 and thus represent the likely interacting domain. Indeed, positive interaction between Tctex-1 and Rab3D aa 74 to 95 was confirmed by subsequent Y-2H analyses (Fig. 1G). Structural and sequence analyses revealed that amino acid residues 74 to 95 (Fig. 1I, QIWDTAGQERYRTITTAYYRGA, yellow underline) map to loops 4 and 5 and the short amphipathic α-2 helix of the Rab3D switch II/GTP-binding motif, a region conserved among Rab3 isoforms (Fig. 1H and I). This region is also notably conserved among other Rab family members thus far not examined, including Rab1 and Rab8, hinting that Tctex-1 may interact with multiple Rab isoforms as observed with most Rab effectors (9).

***In vivo* interaction between Rab3D and Tctex-1 is GTP dependent.** The binding of Tctex-1 to the switch II region of Rab3D implied that the Tctex-1 interaction may be dependent on the guanine nucleotide (GDP/GTP) status of Rab3D, a feature characteristic of all *bona fide* Rab effector molecules. Consistent with this position, coimmunoprecipitation experiments using Myc-tagged wild-type Rab3A, -B, -C, and -D and FLAG–Tctex-1 loaded with either GDP or GTP[γS], a nonhydrolyzable form of GTP, revealed that Tctex-1 preferentially interacted with Rab3D and other Rab3 family members alike, when locked in its GTP-bound form (Fig. 2A). This GTP

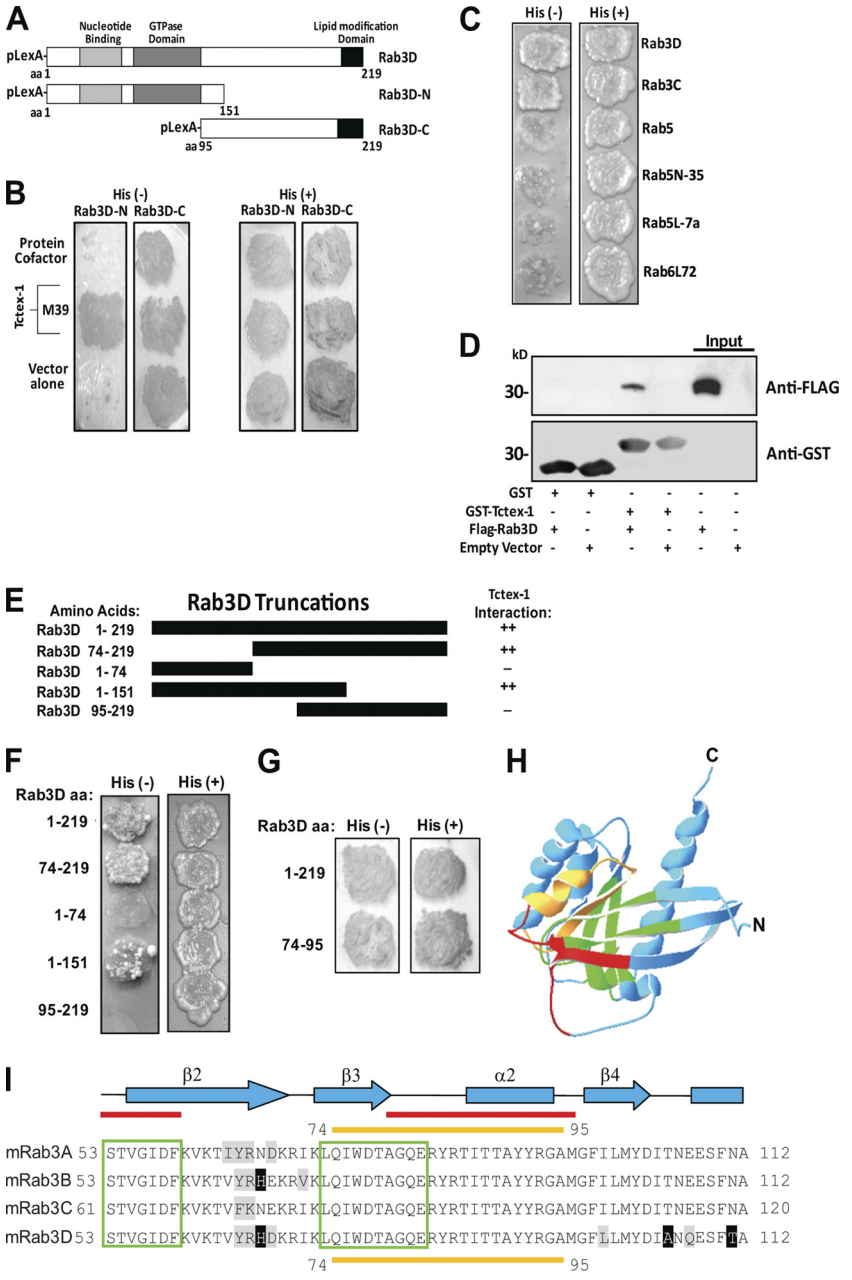

FIG. 1. Identification of Tctex-1 as Rab3D binding protein. (A) Schematic representation of Rab3D N-terminal (aa 1 to 151) and C-terminal (aa 95 to 219) pBTM116 bait constructs used in the Y-2H screen. (B) Rab3D-N (aa 1 to 151) and Rab3D-C (aa 95 to 219) baits were cotransformed with VP16-protein cofactor (control), VP16–Tctex-1 (clone M39), or VP16 vector alone (control). Identification of positive colonies was detected using histidine-deficient (His^-) plates. (C) Tctex-1 specifically interacts with Rab3 proteins but not other Rab family members. Rab protein bait constructs were tested against the Tctex-1 prey in the Y-2H system for their ability to grow on selective medium (His^-), compared to nonselective medium (His^+). (D) Interaction between Tctex-1 and Rab3D. GST–Tctex-1 fusion protein or GST protein alone bound to glutathione-Sepharose beads were incubated with lysate from COS-1 cells transfected with either FLAG-Rab3D or an empty control vector. Bead-bound proteins were detected by immunoblotting using anti-GST antibodies, stripped, and reprobed with antibodies against FLAG. Respective FLAG-Rab3D and control inputs are indicated. (E and F) Mapping the Tctex-1 binding domain of Rab3D. Schematic of bait constructs used to identify the Tctex-1 binding domain of Rab3D. Truncation mutants of Rab3D were tested as LexA fusions for interaction with VP16–Tctex-1 by Y-2H analysis on selective medium (His^-). Magnitudes of β-galactosidase reporter activation are indicated (++, strong; −, not detected). (G) Rab3D aa 74 to 95 represent the minimal binding domain for Tctex-1 interaction by Y-2H analysis. (H) Tctex-1 binds to the switch II domain of Rab3D. Ribbon diagram of the Rab3D backbone (adapted from reference 27 with permission of the publisher). Tctex-1 binding domain is highlighted in yellow, red corresponds to switch domains, green denotes conserved G1 to G5 regions, and blue highlights the remaining backbone residues. (I) Multiple amino acid sequence alignment of mouse (m) Rab3 GTPases. Conserved amino acids appear black on a white background, and Tctex-1 binding/Rab3 switch II domain (aa 74 to 95) is underscored by a yellow line. Red lines overlap the switch domains, and green boxes correspond to the Rab3 G1 to G5 domains.

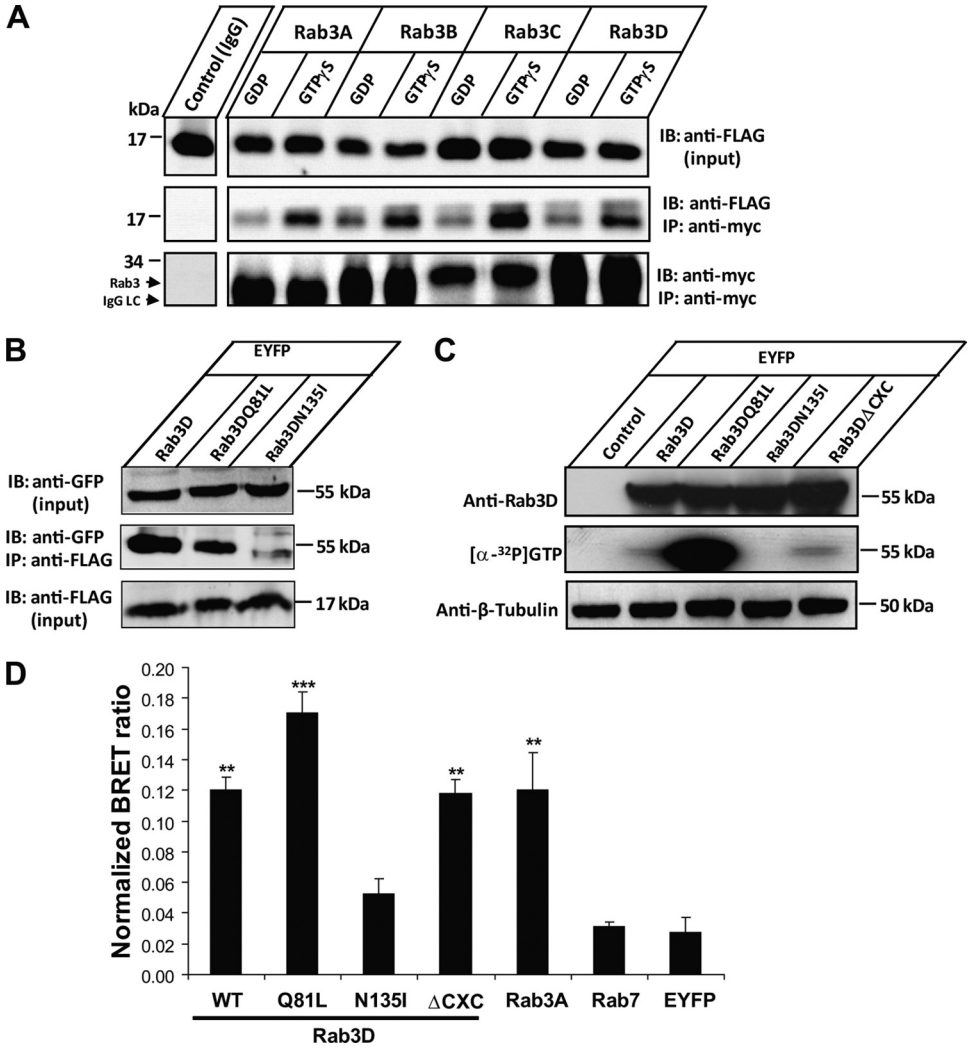

FIG. 2. Tctex-1 binds Rab3D in a GTP-dependent manner. (A) Coimmunoprecipitation of Tctex-1 with Rab3D and other Rab3 family members. COS-1 cells were transiently cotransfected with FLAG–Tctex-1 and Myc-Rab3(A/B/C/D), and lysates (loaded with either GDP or nonhydrolyzable GTP[γS]) were subjected to immunoprecipitation (IP) using an antibody against the Myc epitope. Captured immune complexes were eluted and immunoblotted (IB) with antibodies against FLAG or Myc. Blots are representative of three independent experiments. (B) Coimmunoprecipitation of Tctex-1 with Rab3D wild type and GTP-hydrolysis/-binding mutants. COS-1 cells cotransfected with FLAG–Tctex-1 and either EYFP-tagged Rab3D wild type or constitutively active (Q81L) or inactive (N135I) Rab3D mutants were subjected to immunoprecipitation using an anti-FLAG antibody. Captured immune complexes were eluted and immunoblotted with antibodies against GFP. Blots are representative of three independent experiments. (C) GTP-binding affinity of EYFP-tagged Rab3D wild type and constitutively active (Q81L), inactive (N135I), and prenylation-deficient (ΔCXC) mutants in COS-1 cells. (D) BRET between Tctex-1 and Rab3D. COS-1 cells were transiently cotransfected with Rluc–Tctex-1 (donor) and either EYFP-tagged (acceptor) $Rab3D^{wt}$, $Rab3D^{Q81L}$, $Rab3D^{N135I}$, $Rab3D^{\Delta CXC}$, $Rab3A^{wt}$, or $Rab7^{wt}$ constructs. Samples were analyzed for BRET emission, and data are expressed as BRET ratios normalized to Rluc alone. EYFP alone served as a negative control for statistical analyses (*, $P < 0.001$; **, $P < 0.0001$). Data represent the mean from six independent experiments ± standard error of the mean (SEM).

dependence was similarly observed in reverse coimmunoprecipitation experiments using FLAG–Tctex-1 with the EYFP-tagged Rab3D wild type and selective Rab3D mutants deficient in either GTP hydrolysis ($Rab3D^{Q81L}$) or GTP/GDP binding ($Rab3D^{N135I}$) with both the wild-type and constitutively active (Q81L) Rab3D showing strong binding to Tctex-1, with weak coprecipitation observed between Tctex-1 and the nucleotide-empty, and thus inactive, N135I mutant (Fig. 2B and C).

To further probe the guanine nucleotide dependence of the Rab3D–Tctex-1 interaction *in vivo*, we also sought to study whether Tctex-1 showed similar GTP-dependent binding specificity for Rab3D expressed in live mammalian cells using bioluminescence resonance energy transfer (BRET) assays (7). To this end, COS-1 cells were cotransfected with Tctex-1 fused to an Rluc reporter gene together with either EYFP-tagged Rab3A, Rab3D, or Rab7 or Rab3D mutant $Rab3D^{Q81L}$, $Rab3D^{N135I}$, or $Rab3D^{\Delta CXC}$ (prenylation deficient). Consistent with the above data, we found that Tctex-1 strongly bound both Rab3A and Rab3D. This binding was significantly enhanced when Tctex-1 was coexpressed with Rab3D in its "GTP-locked" form ($Rab3D^{Q81L}$). Conversely, the inactive

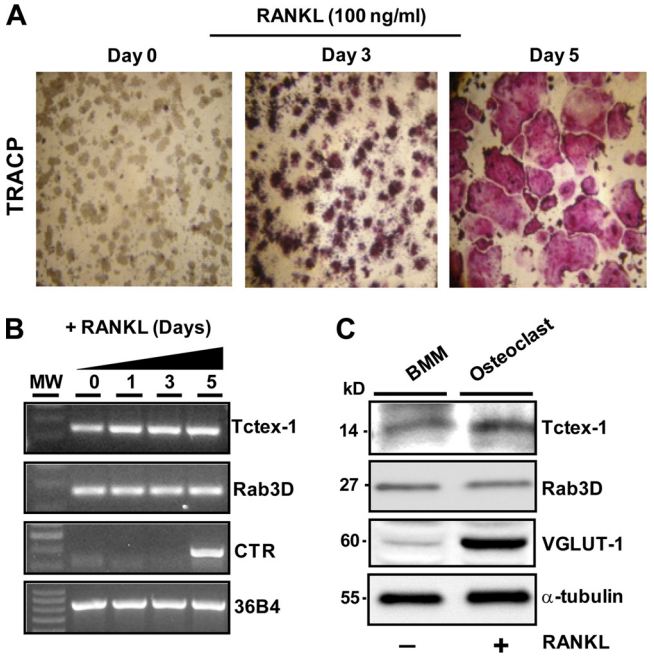

FIG. 3. Expression pattern of Tctex-1 and Rab3D in osteoclastic cells. (A) RAW 264.7 cell macrophages were differentiated from mononuclear precursors into multinucleated TRACP-positive (pink reaction product) osteoclast-like cells following 5 days of RANKL stimulation. (B) mRNA was harvested from indicated time points for RT-PCR analysis using primers specific for Tctex-1, Rab3D, and the mature osteoclast marker calcitonin receptor (CTR). Acidic ribosomal phosphoprotein P0 (36B4) was used as an internal loading control. MW, molecular weight. (C) Protein expression of Tctex-1 and Rab3D in RANKL-differentiated bone marrow monocytes (BMM). M-CSF-dependent mouse BMM were treated in the presence or absence of RANKL to induce osteoclastic cell formation. After 5 days, cells were lysed, and protein was harvested for SDS-PAGE and immunoblotting using antibodies specific to Tctex-1, Rab3D, and the pro-osteoclastic marker vesicular glutamate transporter (VGLUT-1). α-tubulin served as a loading control (20 μg/well). Blots are representative of at least 3 independent experiments.

Rab3D^{N135I} mutant showed low binding to Tctex-1 comparable to but higher than that seen with the controls EYFP alone and Rab7 (Fig. 2D). These findings further indicate that the Rab3D–Tctex-1 interaction is GTP dependent.

Tctex-1 co-occupies Rab3D vesicles in osteoclastic cells. Next, we probed for endogenous Tctex-1–Rab3D expression and subcellular localization in osteoclastic cells. We reasoned that if the GTP–Rab3D–Tctex-1 interaction is physiologically relevant, then the two proteins should not only be coexpressed but also share the same intracellular compartment. Accordingly, RT-PCR analysis using primers specific to mouse Rab3D and Tctex-1 revealed that both mRNA transcripts are constitutively expressed during RANKL-induced differentiation of RAW 264.7 macrophages into TRACP/calcitonin receptor (CTR)-positive osteoclast-like cells (Fig. 3A and B). Similar results were observed at the protein level, with Tctex-1 expression, like that of its Rab3D interaction partner, remaining relatively constant in mouse M-CSF-dependent bone marrow macrophages (BMMs) stimulated in either the presence or absence of RANKL (5-day stimulation) compared to that of vesicular glutamate transporter (VGLUT-1), an established pro-osteoclastic marker (29) (Fig. 3C).

Rab3D has long been recognized as a marker of secretory vesicles and Golgi membranes in a wide range of specialized cells, including osteoclasts (27, 32). Consistently, immunolocalization studies using well-characterized antibodies specific to Rab3D and Tctex-1 demonstrated that Rab3D localizes to small intracellular vesicles particularly evident in the juxtanuclear region and cytoplasm of cultured human osteoclastic cells (Fig. 4A and B), reminiscent of secretory vesicles. Importantly, Tctex-1 immunofluorescence strongly colocalized (yellow signal) with Rab3D-positive vesicles both in the perinuclear and peripheral vicinities, possibly reflecting its association with both nascent and/or recycling secretory vesicle subpopulations. A similar colocalization was observed with highly polarized osteoclasts actively resorbing bone. Figure 4B shows representative XY and XZ projections of an image volume of a resorbing osteoclast doubly immunostained for Rab3D and Tctex-1. A comparative overlay of single-image channels shows that most Rab3D-postive vesicles contain Tctex-1, suggesting that the two proteins coexist on secretory vesicles as an endogenous complex. This position is further supported by biochemical analyses, with Tctex-1 found to cosegregate (Fig. 4C, fractions 9 and 10) and coimmunoprecipitate (Fig. 4D) with Rab3D in subfractionated osteoclastic cells.

Tctex-1–Rab3D interaction links cytoplasmic dynein and microtubules to vesicle transport. As Tctex-1 is an established light chain of the cytoplasmic dynein motor complex (20) and thus a candidate regulator of microtubule-mediated vesicle transport in osteoclasts, we also examined the endogenous localization of Tctex-1 and Rab3D, with respect to cytoplasmic dynein and the microtubule network. First, we compared the sedimentation profiles of Tctex-1 and Rab3D in subfractionated osteoclasts with antibodies against the conventional cytoplasmic dynein intermediate chain (IC74) and α-tubulin. As illustrated in Fig. 4C, peak immunopositive fractions of both Rab3D and Tctex-1 closely comigrated with dynein IC74. Partial overlap between Rab3D–Tctex-1 fractions was also observed with α-tubulin, which exhibited a broad sedimentation profile. Next, we probed for endogenous Rab3D–Tctex-1–dynein–microtubule association by immunofluorescence microscopy. For this purpose, osteoclasts were briefly pre-extracted with microtubule stabilizing buffer to release free cytosolic dynein and Rab3D, fixed, and double immunostained using antibodies against either IC74 or α-tubulin in combination with Tctex-1 and Rab3D. As expected, confocal microscopy revealed strong colocalization between Tctex-1 and its direct dynein-binding partner IC74 (25, 28) in osteoclasts (Fig. 5A). Clear colocalization between dynein IC74 and Rab3D-positive vesicles in osteoclasts actively resorbing bone (Fig. 5B, insets) was also observed. In addition, close association between both Tctex-1 (Fig. 6A) and Rab3D (Fig. 6B) and the microtubule network was observed, with Rab3D vesicles often observed intimately aligning along individual microtubule tracks (Fig. 6B, inset, arrows). Interestingly, this Rab3D–Tctex-1–microtubule coupling could be disrupted following the addition of the microtubule depolymerizing agent nocodazole (Noc), but not other actin (cytochalasin D [cyto D]) or early biosynthetic transport (brefeldin A [BfA]) inhibitors, as evidenced by immunofluorescence microscopy (Fig. 6C) and BRET analyses

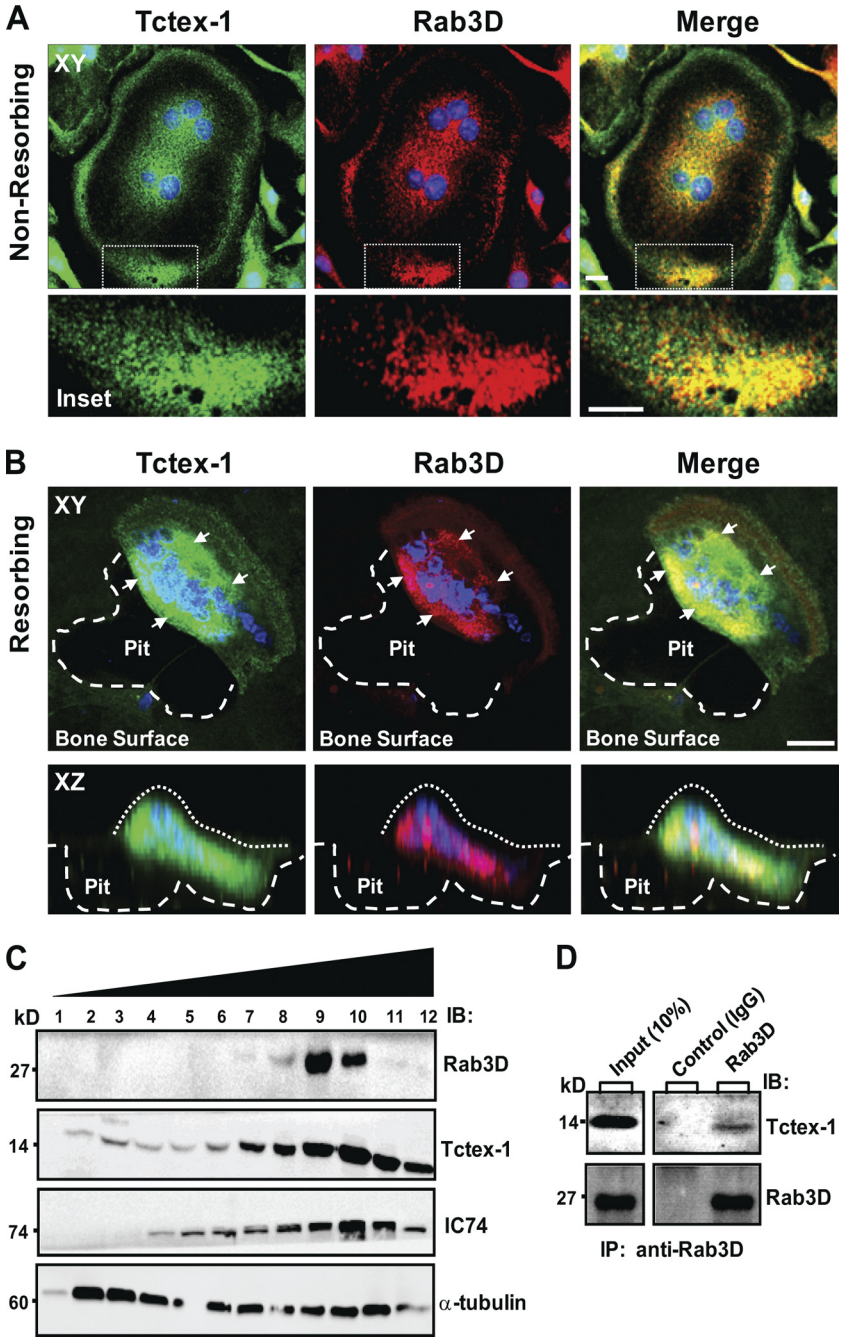

FIG. 4. Tctex-1 co-occupies Rab3D-bearing secretory vesicles in osteoclasts. Primary human osteoclasts were cultured under nonpolarizing or polarizing/bone resorbing conditions, fixed with 4% PFA, immunostained with Tctex-1 and Rab3D antibodies, and examined by laser scanning confocal microscopy. (A) Images are XY projections of a confocal image stack of a nonpolarized osteoclast cultured on glass. Areas of colocalization are depicted in yellow in the merged panel, with nuclei visualized by Hoechst 3342 (blue). Insets indicate magnified views of boxed areas. (B) An image volume of a human osteoclast cultured on cortical bovine bone discs actively resorbing bone in XY and XZ projections. White arrows denote clusters of Tctex-1–Rab3D colocalization. Large white dashes circumscribe the resorptive pit, and small white dashes the osteoclast surface. Bars, 10 μm. (C) Coenrichment of Rab3D and Tctex-1 in subfractionated osteoclasts. Osteoclastic cells were lysed and subjected to velocity density centrifugation (Materials and Methods). Equal volumes of individual fractions were resolved by SDS-PAGE and immunoblotted for Rab3D, Tctex-1, IC74, and α-tubulin. Note that peak fractions of endogenous Rab3D, Tctex-1, and IC74 (fractions 9 and 10) cosediment upon centrifugation. (D) Coimmunoprecipitation of Rab3D–Tctex-1 complexes in osteoclastic cells. Rab3D–Tctex-1 complexes were immunoprecipitated from enriched osteoclastic fractions with either anti-Rab3D or IgG control antibodies, and immunocaptured complexes were resolved by SDS-PAGE and subjected to immunoblot analysis with anti-Rab3D and anti-Tctex-1 antibodies.

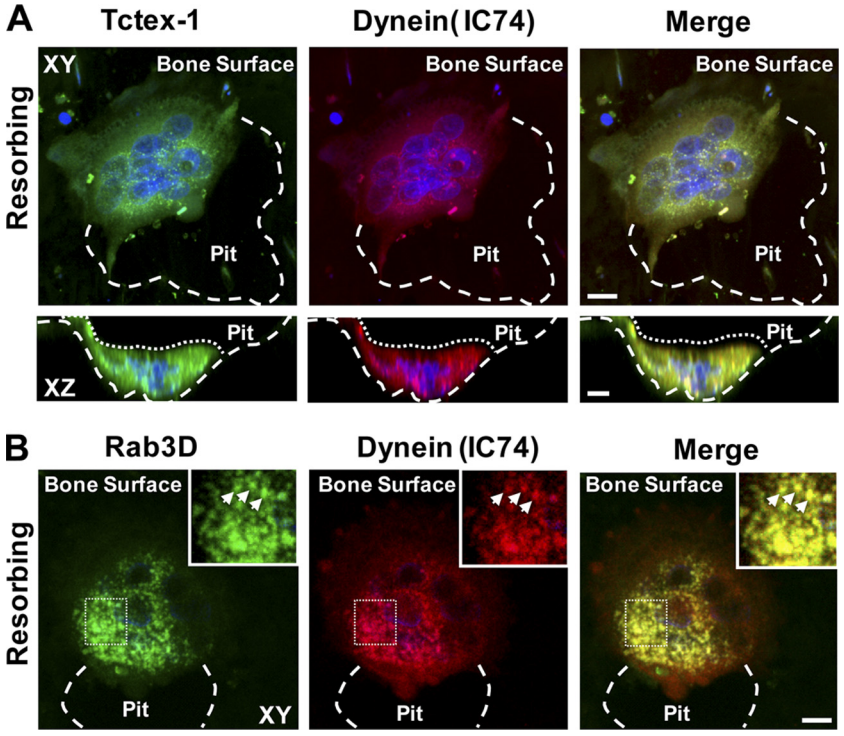

FIG. 5. Tctex-1 and Rab3D colocalize with cytoplasmic dynein in bone-resorbing osteoclasts. Human osteoclasts cultured on cortical bovine bone discs were fixed with ice-cold methanol and double immunolabeled with antibodies against either Tctex-1 (A) or Rab3D (B) in combination with the dynein intermediate chain (IC74). Nuclei (blue) are visualized by Hoechst 3342 staining. Images represent XY and/or XZ projections of confocal image volumes of highly polarized osteoclasts actively resorbing bone. Resorptive pits and osteoclast surfaces are demarcated by large and small white dashes, respectively. Insets in panel B represent magnifications of boxed areas, and arrows depict colocalization on individual fluorescence puncta. Bars, 10 μm.

(Fig. 6D). Taken together, these data imply that Rab3D vesicles associate with cytoplasmic dynein and microtubules, possibly via direct interaction with Tctex-1.

Targeted RNAi ablation of Tctex-1 impairs osteoclastic bone resorption. To explore whether Tctex-1 is a functional requirement of osteoclastic bone resorption, we next devised an RNA interference (RNAi) strategy to specifically suppress Tctex-1 in osteoclasts derived from isolated human peripheral blood monocytes (refer to Materials and Methods). To ensure a sustained level of Tctex-1 suppression during osteoclastogenesis, isolated M-CSF/RANKL-stimulated monocytes were repeatedly transfected with either Tctex-1-targeted or control siRNAs throughout osteoclast differentiation and assayed for Tctex-1 expression levels upon osteoclast maturation. Three independent Tctex-1 siRNAs (denoted TC1 to TC3) and two control siRNAs (negative and GFP) were initially screened for their ability to deplete mRNA expression of Tctex-1. As shown in Fig. 7A and B, whereas the control siRNAs failed to alter the mRNA expression levels of Tctex-1, the specifically targeted Tctex-1 siRNAs exhibited differential Tctex-1 knockdown potential in osteoclastic cells. By far, Tctex-1 siRNA TC1 proved the most potent, achieving consistent Tctex-1 knockdown (>50%) at both the mRNA (Fig. 7A to C) and protein (data available on request) levels during osteoclastogenesis (Fig. 7C) and upon direct delivery into fully mature osteoclastic cells (Fig. 7A and B). siRNA TC3 also showed sustained suppression of Tctex-1 expression levels during osteoclast formation and maturation, albeit to a lesser degree than TC1. On the other hand, Tctex-1 siRNA TC2 was comparatively inefficient and thus excluded from subsequent investigations.

As we had validated the knockdown approach, mature human osteoclasts pretreated with either control (negative) or Tctex-1-targeted siRNAs (TC1 and TC3) were cultured on cortical bone discs for 48 h to assess bone resorption capacity. To our satisfaction, comprehensive analyses of bone resorptive parameters (including resorptive area, depth of pits, and pit volume) revealed a significant decrease in bone resorptive function in osteoclasts treated with Tctex-1 siRNA TC1 compared to the control (Fig. 7D to G). TC3-treated osteoclasts also showed similar decreases in resorptive capacity; however, only pit depth measurements reached statistical significance. Moreover, analysis of medium CTx-1 concentration, a marker of bone resorption, revealed a significant decrease in CTx-1 release in both TC1 and TC3 siRNA knockdown osteoclast cultures, consistent with the reduced pit depth phenotype (Fig. 7H). Importantly, this loss of resorptive function was not simply a reflection of impaired osteoclastogenic potential and/or sealing zone/ruffled border formation as monitored by staining for TRACP (Fig. 8) and F-actin (Fig. 9), respectively. Moreover, this resorption deficiency phenocopies the bone resorption defects observed with osteoclasts lacking Rab3D (32), suggesting that, like Rab3D, Tctex-1 constitutes a functional component of the osteoclastic bone resorptive machinery.

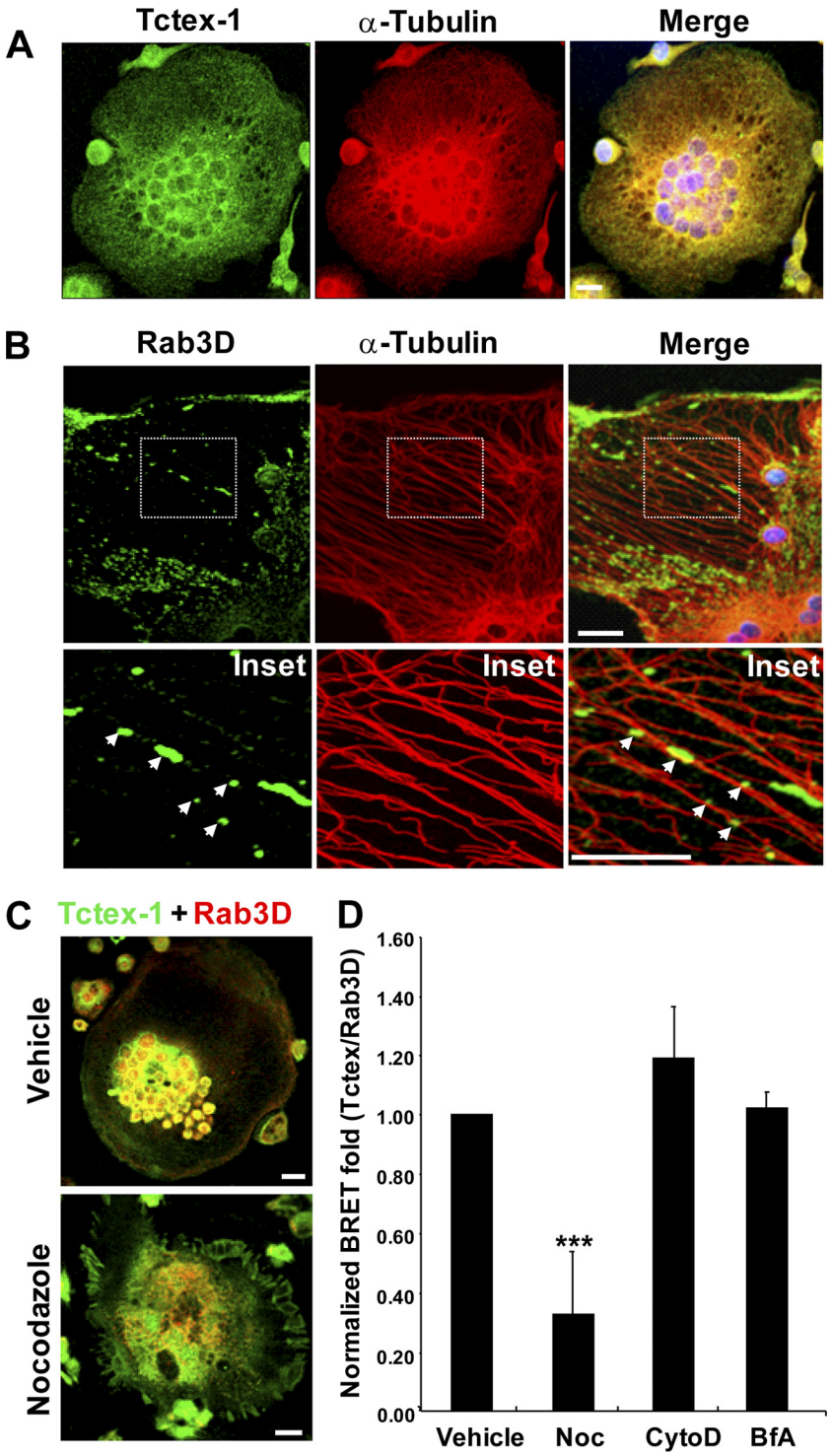

FIG. 6. Colocalization of Tctex-1 and Rab3D with microtubules in osteoclasts and effect of nocodazole on Tctex-1–Rab3D interaction *in vivo*. Osteoclasts were briefly pre-extracted with microtubule stabilizing buffer, fixed in methanol, and then immunostained with the indicated antibodies. (A) A projected XY image stack of an osteoclast stained with anti-Tctex-1 and α-tubulin. (B) A single optical section of an osteoclast stained for anti-Rab3D and α-tubulin. Arrows depict Rab3D-bearing vesicles lying along individual microtubule filaments in magnified insets. (C) Treatment with the microtubule depolymerizing agent nocodazole (2 h) disrupts Rab3D–Tctex-1 distribution in osteoclasts. (D) Effect of brefeldin A, cytochalasin D (cyto D), and nocodazole on Tctex-1–Rab3D interaction as monitored by BRET (***, $P < 0.01$). Data represent the mean from 4 independent experiments ± SEM.

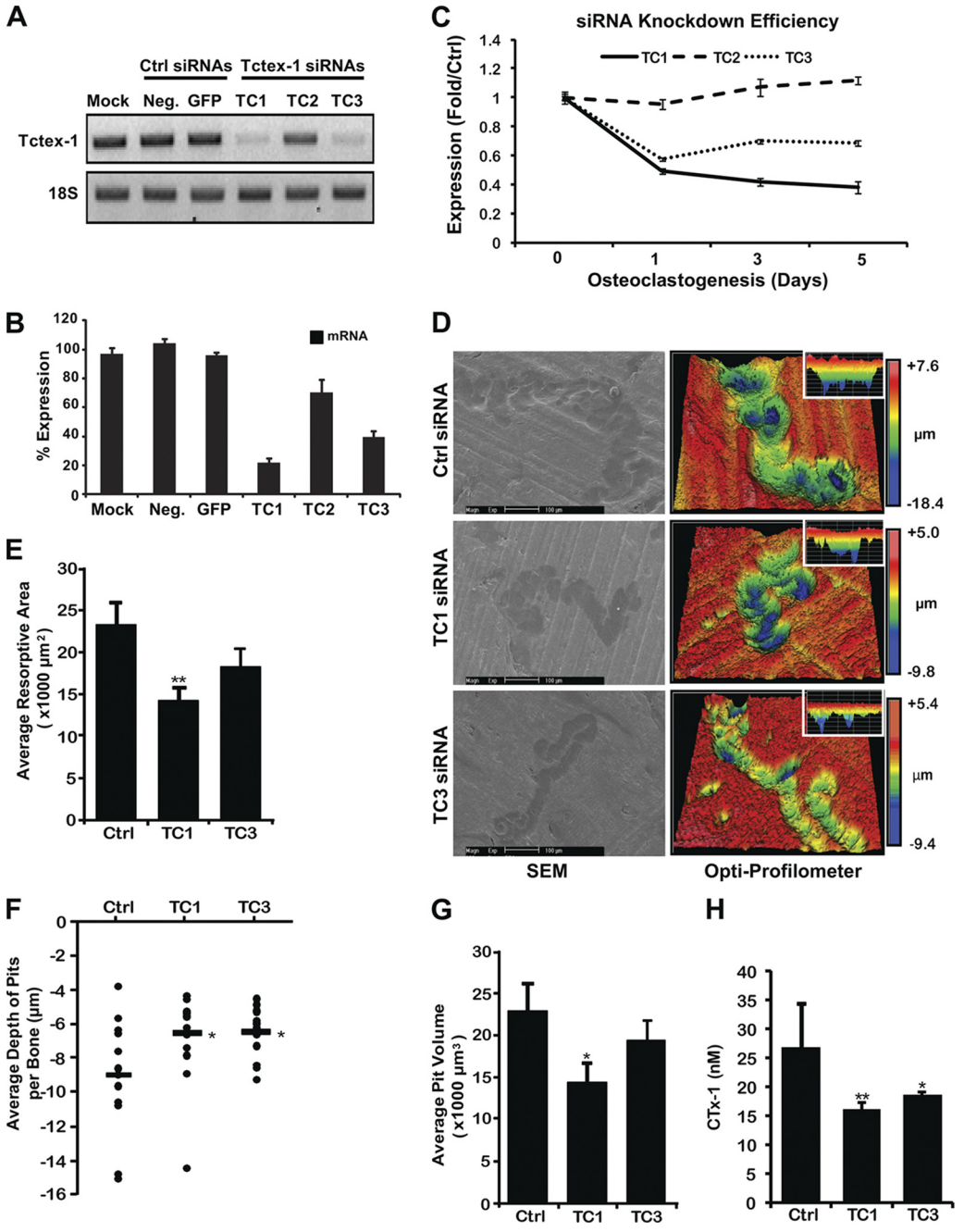

FIG. 7. siRNA-mediated knockdown of Tctex-1 impairs osteoclastic bone resorption *in vitro*. (A, B) Human peripheral blood monocyte (PBMC)-derived mature osteoclasts were transfected with the indicated siRNAs directed against either human Tctex-1 (TC1 to TC3) or control nontargeting siRNAs (negative and GFP) (100 nM), and mRNA levels were examined by semiquantitative RT-PCR. The level of Tctex-1 expression was normalized to that of 18S rRNA and expressed as a percentage of the control. (C) Comparative knockdown efficiency of Tctex-1-targeted siRNAs TC1 to TC3 during osteoclast differentiation. PBMCs were transfected with either Tctex-1 (TC1 to TC3) or control (negative [Ctrl]) siRNAs, and Tctex-1 mRNA levels were directly monitored and compared by semiquantitative RT-PCR during RANKL-induced osteoclastogenesis over 5 days. The level of Tctex-1 expression was normalized to that of 18S rRNA, and data are presented as fold expression over that of the negative siRNA control. (D) Bone resorptive activities of Tctex-1 knockdown PMBC-derived osteoclasts (TC1 and TC3) were determined by culturing osteoclasts at a low density on bovine bone slices for 48 h. Osteoclasts were stained for TRACP, bone slices were assessed by scanning electron microscopy (SEM), and resorptive parameters were quantified. Representative images of resorption pit depths analyzed by SEM (left) and surface texture profilometry on a 3D optical profilometer (Zygo NewView 6300) (right). Note that the individual color scale bars reflect the differing pit depths between Tctex-1 knockdown and control osteoclasts, with pits from Tctex-1 knockdown osteoclasts deemed morphologically shallow. Quantification of the average resorptive area (E), depth (F), and average volume (G) of resorption pits quantified per bone slice from Tctex-1 knockdown and control osteoclasts. (H) The culture media from each 96-well plate were collected, and CTx-1 levels were measured by enzyme-linked immunosorbent assay (ELISA) ($n = 6$). All data are expressed as mean ± SEM and representative of three independent experiments. *, $P < 0.05$; **, $P < 0.01$ versus control.

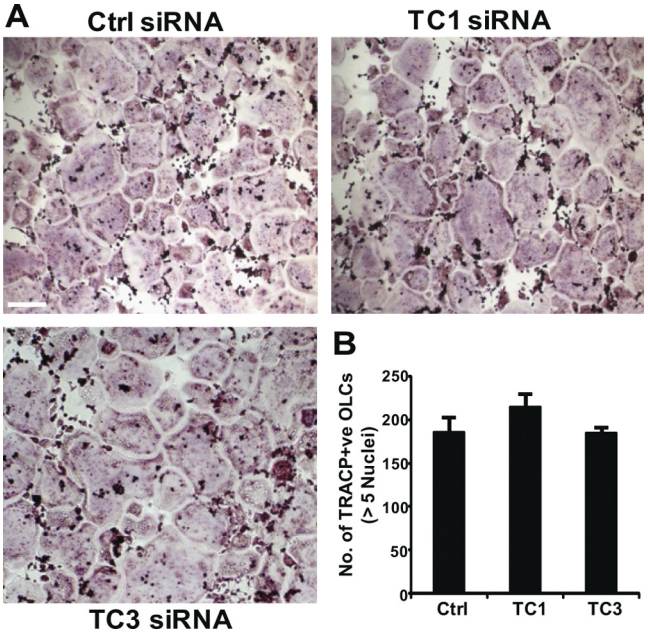

FIG. 8. siRNA-mediated knockdown of Tctex-1 does not affect osteoclastogenesis. M-CSF-dependent monocytes were differentiated in the presence of RANKL and either Tctex-1 (TC1, TC3) or control (Ctrl) siRNAs (100 nM). Following formation, OLCs were stained for TRACP activity (A), and the number of TRACP-positive OLCs with more than 5 nuclei were quantified (B). Data are expressed as mean ± SEM and representative of three independent experiments. Bar, 30 μm.

siRNA knockdown of Tctex-1 mislocalizes Rab3D vesicles during osteoclastic bone resorption. Finally, to gain insight into the mechanism underlying this bone resorption deficiency and potential contribution of Tctex-1 in Rab3D vesicle transport, we examined the effect of siRNA-mediated Tctex-1 knockdown on the subcellular localization of Rab3D during osteoclastic bone resorption. To this end, human osteoclasts grown on bovine bone slices were treated with either control siRNA (negative) or Tctex-1-targeted siRNAs (TC1 and TC3) for 48 h before being fixed and immunostained for Rab3D. In parallel, osteoclasts were stained with rhodamine-conjugated phalloidin to gauge the impact of siRNA treatment on osteoclast F-actin ring formation, a hallmark of osteoclast polarization and ruffled border integrity. As shown in Fig. 9, whereas the control siRNA had no obvious effect on the intracellular distribution of Rab3D, treatment with Tctex-1-targeted siRNAs resulted in a marked mislocalization of Rab3D immunofluorescence. This was particularly evident with the perinuclearly residing Rab3D, which appeared to be redistributed into large vesicular structures in the outer periphery of osteoclasts actively resorbing bone (Fig. 9, arrows). This effect was not an off-target phenomenon, as this mislocalization was observed using two independent Tctex-1 siRNAs (TC1 and TC3). By comparison, little observable differences in the F-actin ring/sealing zone formation between control and Tctex-1 knockdown cells were noted, suggesting that the ruffled border membrane remained largely unaltered. Taken together, these data indicate that Tctex-1 is required to maintain the spatial positioning of Rab3D vesicles during osteoclastic bone resorption.

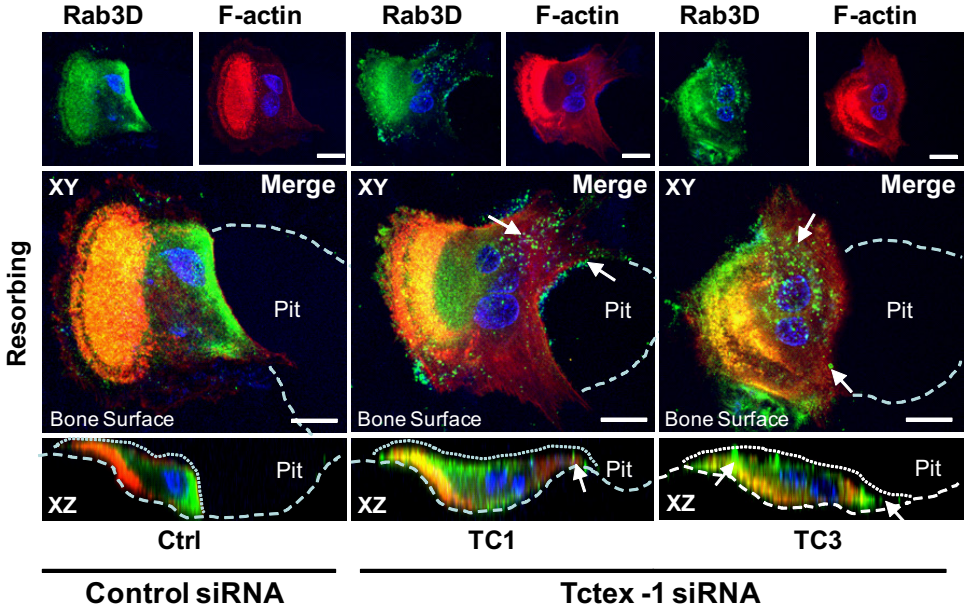

FIG. 9. Tctex-1 knockdown mislocalizes Rab3D-bearing vesicles in bone-resorbing osteoclasts. Human osteoclasts were cultured on bone in the presence of either control (Ctrl) or Tctex-1-targeted siRNAs (TC1 and TC3). After 48 h, osteoclasts were fixed with 4% PFA, immunostained with rhodamine-conjugated phalloidin/F-actin (red) and anti-Rab3D antibodies (green), and examined by laser scanning confocal microscopy. Images are XY and XZ projections of a confocal image stack of human osteoclasts actively resorbing bone, with nuclei visualized by Hoechst 3342 (blue). Note that whereas Rab3D immunofluorescence is localized predominately to the perinuclear vicinity in control siRNA-treated osteoclasts (Ctrl), Rab3D is redistributed markedly to peripheral clusters (white arrows) upon Tctex-1 depletion. Resorptive pits and osteoclast surfaces are demarcated by large and small white dashes, respectively. Bars, 10 μm.

DISCUSSION

Tctex-1 was first identified as a member of a multigene family that maps to the t-complex of mouse chromosome 17 (23) but later shown to encode a versatile light chain of cytoplasmic dynein, serving to link diverse cargos to the dynein motor complex (20, 42–44). More recently, accumulated evidence suggests that Tctex-1 also regulates dynein-independent functions, including G protein signaling (36) and actin remodeling (4), although the significance of these accessory roles remains incompletely understood.

Rab3 proteins represent a highly homologous subfamily of Rab GTPases (Rab3A/B/C/D) which cycle "on" and "off" secretory vesicles, in concert with their activation states (8, 14), and thus are widely considered core components of the mammalian exocytotic release machinery (24). Unlike Rab3A/B/C, which are predominantly expressed in the brain and occupy synaptic vesicles, Rab3D is expressed in nonneuronal cell types with high secretory requirements where it localizes to specialized secretory vesicles (34, 35, 46, 47) and Golgi membranes (14, 48). In bone-resorbing osteoclasts, Rab3D has been implicated in the trafficking of post-TGN vesicles and ruffled border formation (32); however, the downstream effectors through which Rab3D elicits its biological function have, until now, remained elusive. Here we identify Tctex-1 as a new Rab3D-interacting partner and present several novel observations. First, Tctex-1 binds specifically to Rab3D in a GTP-dependent fashion. Second, Tctex-1 coexists endogenously with Rab3D and the cytoplasmic dynein complex on secretory vesicles in bone-resorbing osteoclasts. Third, the Rab3D–Tctex-1 interaction is dependent on the integrity of the microtubule cytoskeleton. Finally, targeted disruption of Tctex-1 impairs osteoclastic bone resorption, an effect that correlates with a redistribution of Rab3D-bearing vesicles. Collectively, these findings document for the first time that Tctex-1 is a novel binding partner of Rab3D in osteoclasts and indicate that Tctex-1, like Rab3D, forms an integral component of the osteoclastic bone resorptive machinery.

The identification of Tctex-1 as a novel Rab3D effector extends Rab3D to the growing list of Rabs known to modulate membrane-cytoskeleton interactions (11, 18). While our *in vitro* and *in vivo* protein-protein interaction studies clearly demonstrate that Tctex-1 binds specifically and GTP dependently to Rab3D/Rab3 family members, at this time we cannot exclude the possibility that Tctex-1 may also interact with additional Rabs which share the highly conserved switch II binding domain. Furthermore, it remains unclear whether Tctex-1 binds directly to Rab3D or inadvertently via a hitherto unknown adaptor molecule that may bridge Rab3D–Tctex-1 pairing with high affinity as observed with other Rab-motor interplays. For instance, Rab6 has been shown to recruit several components of the kinesin (Rabbakinesin-6) (6) and dynein-dynactin microtubule motor complexes (Bicaudal-D [BICD1/2]), $p150^{Glued}$ (10, 26, 39, 52), and DYNLRB1 (52) to Golgi membranes. Similarly, Rab7 has been implicated in the stepwise assembly of the dynein motor complex on late endosomes through the recruitment of a tripartite complex consisting of Rab7 effectors RILP and ORP1L (15–17). These effectors have not been limited to microtubule-based motors, with several Rab-actomyosin interactions also reported, all of which involve class V myosins and myosin adaptors (11).

The impairment of osteoclastic bone resorption by Tctex-1 RNA interference is consistent with previous resorptive deficiencies observed with osteoclasts derived from Rab3D-deficient mice (32), indicating that Tctex-1 might serve as a functional component of the Rab3D vesicle transport machinery. Indeed, disruption in bone resorptive function following Tctex-1 knockdown correlated with a mislocalization of Rab3D vesicles from the perinuclear region to the peripheral vicinity, possibly reflecting the uncoupling of Rab3D vesicle transport from cytoplasmic dynein upon Tctex-1 depletion. While the observed disruption in resorption activity is far from complete, it may simply reflect the incomplete Tctex-1 knockdown efficiency attained using siRNAs in mature osteoclasts. Alternatively, it might indicate that the loss of Tctex-1 alone is not sufficient to block all Rab3D trafficking, hinting that other effector proteins, which functionally compensate and/or reroute this trafficking pathway, may exist. The future characterization of Tctex-1 knockout mice, together with the identification of additional Rab3D effectors, will therefore be crucial toward establishing the precise physiological relevance of this Rab-motor association.

How might Tctex-1 modulate Rab3D vesicle transport during osteoclastic bone resorption? In the absence of further experiments, we can only speculate as to the exact molecular basis behind the Rab3D–Tctex-1 interaction. Nevertheless, based on the contemporary view of the Rab-motor interactions together with the data presented here, we envisage a tempting scenario whereby Tctex-1 is actively recruited to Rab3D-bearing vesicles in osteoclasts during bone resorption. According to this position, Tctex-1 would serve as a molecular adaptor for the dynein motor complex, linking Rab3D vesicles to microtubules and thus bridging membrane-microtubule transport during bone resorption. Given that Tctex-1 interaction is dependent on the guanine nucleotide status of Rab3D, inactivation of Rab3D (via GTP hydrolysis) may catalyze the disassembly of this Rab-motor complex, thus enabling Rab3D to engage with additional effectors that may be required for successive stages of vesicle transport. In this way, Rab3D-mediated vesicle transport would be dependent on cycles of GTP binding and hydrolysis, consistent with the "molecular switch" hypothesis.

Given that cytoplasmic dynein is a minus-end-directed microtubule motor, it is likely that Tctex-1 serves to facilitate the retrograde recycling and spatial positioning of Rab3D-bearing secretory vesicles during osteoclastic bone resorption. The observed mislocalization of Rab3D vesicles upon Tctex-1 knockdown would be consistent with this position. Another far reaching possibility is that Rab3D–Tctex-1 participates in a transcytotic pathway from the ruffled border to opposing basolateral domains, as occurs with degraded bone matrix substrates during bone resorption (31, 37).

Finally, considering the fundamental role(s) of Rab3D in other secretory systems (27), we speculate that the Rab3D–Tctex-1 interaction may also have functional implications that go well beyond the osteoclast field. For instance, in the case of polarized secretory epithelial cells, which possess opposing noncentrosomal apico-basolateral microtubule arrays (i.e., microtubule minus ends face the apical membrane and plus ends face the basal domain), Rab3D–Tctex-1 might function to traf-

fic post-Golgi secretory vesicles toward the apical plasmalemma during regulated exocytosis. Indeed, cytoplasmic dynein has been implicated in the microtubule-directed targeting and positioning of Rab3D-enriched secretory granules to apical lumens of pancreatic and lacrimal acinar cells (21, 49, 51). Similarly, Tctex-1 has been shown to facilitate the minus-end motility of post-Golgi rhodopsin-bearing vesicles to the apical surface in polarized epithelial cells (43) and to the apical surface of the inner segment of light-sensing photoreceptor cells (42) which express Rab3B and Rab3A, respectively (22). Therefore, the identification of Tctex-1 as a novel Rab3D/Rab3-interacting partner may provide a molecular basis for these observations and thus may open up several lines of future investigation.

ACKNOWLEDGMENTS

We thank R. Regazzi, S. M. King, M. Zerial, and S. P. Klinken for providing antibodies and cDNA constructs. All microscopy was carried out using facilities at the Centre for Microscopy, Characterization, and Analysis, The University of Western Australia. We thank Karin Eidne for assisting with BRET assays and Adrian Keating for his assistance with the optical profilometer as well as the Australian Research Council for support of this instrument (LE0775499).

This work was supported by the National Health and Medical Research Council of Australia (NHMRC, ID458765) to M.-H.Z., J.X., and N.J.P., the UWA Research Scheme to N.J.P., and the Raine Foundation to N.J.P. N.J.P. is a NHMRC CJ Martin Fellow (ID463911). J.X. is a recipient of the ASBMR Career Enhancement Award. This work was further supported by the NIH (EY11307) and Research To Prevent Blindness to C.-H.S.

REFERENCES

1. **Abu-Amer, Y., S. L. Teitelbaum, J. C. Chappel, P. Schlesinger, and F. P. Ross.** 1999. Expression and regulation of RAB3 proteins in osteoclasts and their precursors. J. Bone Miner. Res. **14:**1855–1860.
2. **Bucci, C., P. Thomsen, P. Nicoziani, J. McCarthy, and B. van Deurs.** 2000. Rab7: a key to lysosome biogenesis. Mol. Biol. Cell **11:**467–480.
3. **Campbell, K. S., S. Cooper, M. Dessing, S. Yates, and A. Buder.** 1998. Interaction of p59fyn kinase with the dynein light chain, Tctex-1, and colocalization during cytokinesis. J. Immunol. **161:**1728–1737.
4. **Chuang, J. Z., et al.** 2005. The dynein light chain Tctex-1 has a dynein-independent role in actin remodeling during neurite outgrowth. Dev. Cell **9:**75–86.
5. **Coxon, F. P., and A. Taylor.** 2008. Vesicular trafficking in osteoclasts. Semin. Cell Dev. Biol. **19:**424–433.
6. **Echard, A., et al.** 1998. Interaction of a Golgi-associated kinesin-like protein with Rab6. Science **279:**580–585.
7. **Feng, H., et al.** 2008. Cytoplasmic terminus of a vacuolar type proton pump accessory subunit Ac45 is required for proper interaction with V0 domain subunits and efficient osteoclastic bone resorption. J. Biol. Chem. **283:**13194–13204.
8. **Fischer von Mollard, G., T. C. Sudhof, and R. Jahn.** 1991. A small GTP-binding protein dissociates from synaptic vesicles during exocytosis. Nature **349:**79–81.
9. **Fukuda, M., E. Kanno, K. Ishibashi, and T. Itoh.** 2008. Large-scale screening for novel Rab effectors reveals unexpected broad Rab-binding specificity. Mol. Cell. Proteomics **7:**1031–1042.
10. **Grigoriev, I., et al.** 2007. Rab6 regulates transport and targeting of exocytotic carriers. Dev. Cell **13:**305–314.
11. **Hammer, J. A., III, and X. S. Wu.** 2002. Rabs grab motors: defining the connections between Rab GTPases and motor proteins. Curr. Opin. Cell Biol. **14:**69–75.
12. **Huang, L., J. Xu, D. J. Wood, and M. H. Zheng.** 2000. Gene expression of osteoprotegerin ligand, osteoprotegerin, and receptor activator of NF-kappaB in giant cell tumor of bone: possible involvement in tumor cell-induced osteoclast-like cell formation. Am. J. Pathol. **156:**761–767.
13. **Iezzi, M., et al.** 1999. Subcellular distribution and function of Rab3A, B, C, and D isoforms in insulin-secreting cells. Mol. Endocrinol. **13:**202–212.
14. **Jena, B. P., et al.** 1994. Redistribution of a rab3-like GTP-binding protein from secretory granules to the Golgi complex in pancreatic acinar cells during regulated exocytosis. J. Cell Biol. **124:**43–53.
15. **Johansson, M., M. Lehto, K. Tanhuanpaa, T. L. Cover, and V. M. Olkkonen.** 2005. The oxysterol-binding protein homologue ORP1L interacts with Rab7 and alters functional properties of late endocytic compartments. Mol. Biol. Cell **16:**5480–5492.
16. **Johansson, M., et al.** 2007. Activation of endosomal dynein motors by stepwise assembly of Rab7-RILP-p150^{Glued}, ORP1L, and the receptor βIII spectrin. J. Cell Biol. **176:**459–471.
17. **Jordens, I., et al.** 2001. The Rab7 effector protein RILP controls lysosomal transport by inducing the recruitment of dynein-dynactin motors. Curr. Biol. **11:**1680–1685.
18. **Jordens, I., M. Marsman, C. Kuijl, and J. Neefjes.** 2005. Rab proteins, connecting transport and vesicle fusion. Traffic **6:**1070–1077.
19. **Kim, H., et al.** 2007. Microtubule binding by dynactin is required for microtubule organization but not cargo transport. J. Cell Biol. **176:**641–651.
20. **King, S. M., et al.** 1996. The mouse t-complex-encoded protein Tctex-1 is a light chain of brain cytoplasmic dynein. J. Biol. Chem. **271:**32281–32287.
21. **Kraemer, J., F. Schmitz, and D. Drenckhahn.** 1999. Cytoplasmic dynein and dynactin as likely candidates for microtubule-dependent apical targeting of pancreatic zymogen granules. Eur. J. Cell Biol. **78:**265–277.
22. **Kwok, M. C., J. M. Holopainen, L. L. Molday, L. J. Foster, and R. S. Molday.** 2008. Proteomics of photoreceptor outer segments identifies a subset of SNARE and Rab proteins implicated in membrane vesicle trafficking and fusion. Mol. Cell. Proteomics **7:**1053–1066.
23. **Lader, E., H. S. Ha, M. O'Neill, K. Artzt, and D. Bennett.** 1989. tctex-1: a candidate gene family for a mouse t complex sterility locus. Cell **58:**969–979.
24. **Lang, T., and R. Jahn.** 2008. Core proteins of the secretory machinery. Handb. Exp. Pharmacol. **184:**107–127.
25. **Makokha, M., M. Hare, M. Li, T. Hays, and E. Barbar.** 2002. Interactions of cytoplasmic dynein light chains Tctex-1 and LC8 with the intermediate chain IC74. Biochemistry **41:**4302–4311.
26. **Matanis, T., et al.** 2002. Bicaudal-D regulates COPI-independent Golgi-ER transport by recruiting the dynein-dynactin motor complex. Nat. Cell Biol. **4:**986–992.
27. **Millar, A. L., N. J. Pavlos, J. Xu, and M. H. Zheng.** 2002. Rab3D: a regulator of exocytosis in non-neuronal cells. Histol. Histopathol. **17:**929–936.
28. **Mok, Y. K., K. W. Lo, and M. Zhang.** 2001. Structure of Tctex-1 and its interaction with cytoplasmic dynein intermediate chain. J. Biol. Chem. **276:**14067–14074.
29. **Morimoto, R., et al.** 2006. Secretion of L-glutamate from osteoclasts through transcytosis. EMBO J. **25:**4175–4186.
30. **Mulari, M., J. Vaaraniemi, and H. K. Vaananen.** 2003. Intracellular membrane trafficking in bone resorbing osteoclasts. Microsc. Res. Tech. **61:**496–503.
31. **Nesbitt, S. A., and M. A. Horton.** 1997. Trafficking of matrix collagens through bone-resorbing osteoclasts. Science **276:**266–269.
32. **Pavlos, N. J., et al.** 2005. Rab3D regulates a novel vesicular trafficking pathway that is required for osteoclastic bone resorption. Mol. Cell. Biol. **25:**5253–5269.
33. **Pfister, K. K., et al.** 2005. Cytoplasmic dynein nomenclature. J. Cell Biol. **171:**411–413.
34. **Raffaniello, R. D., J. Lin, R. Schwimmer, and G. K. Ojakian.** 1999. Expression and localization of Rab3D in rat parotid gland. Biochim. Biophys. Acta **1450:**352–363.
35. **Riedel, D., et al.** 2002. Rab3D is not required for exocrine exocytosis but for maintenance of normally sized secretory granules. Mol. Cell. Biol. **22:**6487–6497.
36. **Sachdev, P., et al.** 2007. G protein beta gamma subunit interaction with the dynein light-chain component Tctex-1 regulates neurite outgrowth. EMBO J. **26:**2621–2632.
37. **Salo, J., P. Lehenkari, M. Mulari, K. Metsikko, and H. K. Vaananen.** 1997. Removal of osteoclast bone resorption products by transcytosis. Science **276:**270–273.
38. **Sambrook, J., E. F. Fritsch, and T. Maniatis.** 1989. Molecular cloning: a laboratory manual, 2nd ed. Cold Spring Harbor Laboratory Press, Cold Spring Harbor, NY.
39. **Short, B., C. Preisinger, J. Schaletzky, R. Kopajtich, and F. A. Barr.** 2002. The Rab6 GTPase regulates recruitment of the dynactin complex to Golgi membranes. Curr. Biol. **12:**1792–1795.
40. **Stenmark, H.** 2009. Rab GTPases as coordinators of vesicle traffic. Nat. Rev. Mol. Cell Biol. **10:**513–525.
41. **Sun, Y., K. G. Buki, O. Ettala, J. P. Vaaraniemi, and H. K. Vaananen.** 2005. Possible role of direct Rac1-Rab7 interaction in ruffled border formation of osteoclasts. J. Biol. Chem. **280:**32356–32361.
42. **Tai, A. W., J. Z. Chuang, C. Bode, U. Wolfrum, and C. H. Sung.** 1999. Rhodopsin's carboxy-terminal cytoplasmic tail acts as a membrane receptor for cytoplasmic dynein by binding to the dynein light chain Tctex-1. Cell **97:**877–887.
43. **Tai, A. W., J. Z. Chuang, and C. H. Sung.** 2001. Cytoplasmic dynein regulation by subunit heterogeneity and its role in apical transport. J. Cell Biol. **153:**1499–1509.
44. **Tai, A. W., J. Z. Chuang, and C. H. Sung.** 1998. Localization of Tctex-1, a cytoplasmic dynein light chain, to the Golgi apparatus and evidence for dynein complex heterogeneity. J. Biol. Chem. **273:**19639–19649.

45. **Teitelbaum, S. L.** 2007. Osteoclasts: what do they do and how do they do it? Am. J. Pathol. **170:**427–435.
46. **Tuvim, M. J., et al.** 1999. Rab3D, a small GTPase, is localized on mast cell secretory granules and translocates to the plasma membrane upon exocytosis. Am. J. Respir. Cell Mol. Biol. **20:**79–89.
47. **Valentijn, J. A., et al.** 1996. Rab3D localizes to secretory granules in rat pancreatic acinar cells. Eur. J. Cell Biol. **70:**33–41.
48. **Valentijn, J. A., L. van Weeren, A. Ultee, and A. J. Koster.** 2007. Novel localization of Rab3D in rat intestinal goblet cells and Brunner's gland acinar cells suggests a role in early Golgi trafficking. Am. J. Physiol. Gastrointest. Liver Physiol. **293:**G165–G177.
49. **Valentijn, K., J. A. Valentijn, and J. D. Jamieson.** 1999. Role of actin in regulated exocytosis and compensatory membrane retrieval: insights from an old acquaintance. Biochem. Biophys. Res. Commun. **266:**652–661.
50. **Van Wesenbeeck, L., et al.** 2007. Involvement of PLEKHM1 in osteoclastic vesicular transport and osteopetrosis in *incisors absent* rats and humans. J. Clin. Invest. **117:**919–930.
51. **Wang, Y., et al.** 2003. Cytoplasmic dynein participates in apically targeted stimulated secretory traffic in primary rabbit lacrimal acinar epithelial cells. J. Cell Sci. **116:**2051–2065.
52. **Wanschers, B. F., et al.** 2007. A role for the Rab6B Bicaudal-D1 interaction in retrograde transport in neuronal cells. Exp. Cell Res. **313:**3408–3420.
53. **Xu, J., T. Cheng, H. T. Feng, N. J. Pavlos, and M. H. Zheng.** 2007. Structure and function of V-ATPases in osteoclasts: potential therapeutic targets for the treatment of osteolysis. Histol. Histopathol. **22:**443–454.
54. **Xu, J., et al.** 2000. Cloning, sequencing, and functional characterization of the rat homologue of receptor activator of NF-kappaB ligand. J. Bone Miner. Res. **15:**2178–2186.
55. **Zaidi, M.** 2007. Skeletal remodeling in health and disease. Nat. Med. **13:**791–801.
56. **Zerial, M., and H. McBride.** 2001. Rab proteins as membrane organizers. Nat. Rev. Mol. Cell Biol. **2:**107–117.
57. **Zhao, H., et al.** 2010. How do bone cells secrete proteins? Adv. Exp. Med. Biol. **658:**105–109.
58. **Zhao, H., et al.** 2008. Synaptotagmin VII regulates bone remodeling by modulating osteoclast and osteoblast secretion. Dev. Cell **14:**914–925.
59. **Zhao, H., T. Laitala-Leinonen, V. Parikka, and H. K. Vaananen.** 2001. Downregulation of small GTPase Rab7 impairs osteoclast polarization and bone resorption. J. Biol. Chem. **276:**39295–39302.